

MICROLENSING OF LENSED SUPERNOVAE

GREGORY DOBLER¹ & CHARLES R. KEETON²

Accepted in ApJ

ABSTRACT

Given the number of recently discovered galaxy-galaxy lens systems, we anticipate that a gravitationally lensed supernova will be observed within the next few years. We explore the possibility that stars in the lens galaxy will produce observable microlensing fluctuations in lensed supernova light curves. For typical parameters, we predict that $\sim 70\%$ of lensed SNe will show microlensing fluctuations > 0.5 mag, while $\sim 25\%$ will have fluctuations > 1 mag. Thus microlensing of lensed supernova will be both ubiquitous and observable. Additionally, we show that microlensing fluctuations will complicate measurements of time delays from multiply imaged supernovae: time delays accurate to better than a few days will be difficult to obtain. We also consider prospects for extracting the lens galaxy's stellar mass fraction and mass function from microlensing fluctuations via a new statistical measure, the time-weighted light curve derivative.

Subject headings: gravitational lensing – galaxies: stellar content – supernovae: general

1. INTRODUCTION

Within the past year there has been an explosion in the number of known galaxy-galaxy strong lens systems due to the success of the Sloan Lens ACS (SLACS) survey (Bolton et al. 2004, 2006; Treu et al. 2006; Koopmans et al. 2006). The lens galaxies consist of a subset of the Sloan Digital Sky Survey (SDSS) Luminous Red Galaxy (LRG) catalog (Eisenstein et al. 2001) and were initially selected based on the presence of several “rogue” oxygen emission lines in the otherwise well characterized LRG spectra (Bolton et al. 2004). The hypothesis that these emission features originated from an unresolved background galaxy within the $3''$ SDSS fiber suggested a substantial probability of lensing. Follow-up HST snapshots with the ACS camera revealed that many of the source galaxies are in fact lensed (Bolton et al. 2004, 2006).

Oxygen emission lines trace star formation in both the local and distant universe (Kennicutt 1992; Hogg et al. 1998), so it seems likely that the SLACS sources are undergoing intense star formation. Coupled with the sheer number of lenses discovered with SLACS (~ 30 at present count), this opens up the exciting possibility of observing lensed supernovae (SNe) in the near future.

Lensed SNe offer a variety of interesting applications. For example, Oguri & Kawano (2003) showed that SN magnification distributions can be used to break the degeneracy between the density profile of the lens galaxy and the measured value of the Hubble constant. Cooray et al (2006) investigated the possibility of using weakly lensed SNe to map out large-scale density fluctuations in the universe. Kolatt & Bartelmann (1998) proposed the use of SN magnification distributions to eliminate the mass-sheet degeneracy in cluster mass reconstruction. In this paper, we point out that strongly lensed SNe will also be *microlensed* by the stars in the lens galaxy, and demonstrate that the microlensing fluc-

tuations will contain valuable information about the stellar population of the lens galaxy.

The first lensed SN to be discovered will probably be Type II, as opposed to the Type Ia SNe used to measure the expansion history of the universe (Riess et al 1998; Perlmutter et al 1999; Tonry et al 2003; Knop et al 2003; Riess et al 2004). While SNe II appear to be somewhat less common than SNe Ia when averaged over galaxies of all Hubble types, SNe II have a higher rate among spiral and irregular galaxies (Kennicutt 1992; Mannucci et al 2005). The presence of [O II] emission lines in the SLACS sources suggests that they are predominantly gas-rich spirals and irregulars. Since star forming galaxies typically host one SN II every 50–100 years (Mannucci et al 2005), we expect a SN II to be observed in one of the ~ 30 SLACS source galaxies within the next several years. Although there is scatter among the peak brightnesses of SN II's, the mean B-band luminosity is approximately $M_B \sim -17.5$ (Young & Branch 1989). This implies an apparent magnitude of a SN in the SLACS source population (which has a mean redshift of $z_s \approx 0.53$) of $m \sim 24.5$. Since there is an additional amplification $\mu_0 \sim 10$ due to the main lens galaxy, the apparent magnitude for multiply imaged SNe in the SLACS sample should be $m \sim 22$, a value that is certainly within reach of existing telescopes with reasonable exposure times.

In the SLACS sample, discoveries of lensed SNe will come from monitoring known lens systems. The complementary approach is to mine a catalog of observed SNe to find those that are lensed. This approach could be used with the Supernova Acceleration Probe (SNAP; Aldering et al. 2004, also <http://snap.lbl.gov>), which is intended to observe ~ 2000 – 3000 SNe Ia per year down to 26–27th magnitude. Oguri, Suto, & Turner (2003) forecast that SNAP will discover 2–20 lensed SNe Ia per year, with the uncertainties due mainly to the star formation rate at high redshift. Although SNAP will focus on SNe Ia, the deep imaging will naturally reveal many SNe II as well, raising the total number of lensed SNe by a factor of ~ 2 .

While there are many categories and subcategories of observed SNe (see Filippenko 1997, for a thorough re-

¹ Department of Physics and Astronomy, University of Pennsylvania, 209 S. 33rd Street, Philadelphia, PA 19104 USA

² Department of Physics and Astronomy, Rutgers University, 136 Frelinghuysen Road, Piscataway, NJ 08854 USA

view), the physics behind SN explosions has been studied extensively and both light curves and spectra are reasonably well reproduced in simulations (Eastman et al 1994; Eastman, Schmidt, & Kirshner 1996). The progenitors of SNe II are thought to be massive ($\gtrsim 8\text{--}10 M_{\odot}$; Leonard et al 2001) stars that undergo core collapse when the amount of energy released in fusion reactions is no longer sufficient to counteract self-gravitational forces. The resulting explosion creates an expanding envelope that can be modeled with the Expanding Photosphere Method (Kirshner & Kwan 1974). Light curves of some SN II have been observed with time sampling approaching 1 day (e.g., SN1999em; Leonard et al 2001).

Light that reaches us from a distant SN will of course be affected by all intervening matter, such as dust and gas, leading to photometric and spectroscopic differences between the intrinsic and observed light. Lensed SNe are unique in that they may also exhibit gravitationally induced variability due to intervening stars lying within the lens galaxy. This phenomenon known as microlensing is familiar from quasar lensing, with the best known example being Q2237+030 (Woźniak et al. 2000). The brightnesses of the lensed images fluctuate on time scales of months to years due to relative motion of the lens galaxy and source quasar. For a detailed example of microlensing light curve analysis see Kochanek (2004), and for detailed treatments of quasar microlensing theory see Wytke & Turner (2001); Schechter & Wambsganss (2002); Schechter et al. (2004).

In a microlensed SN, by contrast, what changes with time is the *size* of the source.³ The effects of source size in microlensing have been studied (e.g., Mortonson et al. 2004; Dobler, Keeton, & Wambsganss 2005), with the general conclusion that the amplitude of microlensing fluctuations decreases with increasing source size. Thus, we naïvely expect that microlensing fluctuations may start out large and decrease in amplitude as the SN expands. Another qualitative result is that large sources are not very sensitive to microlensing by small stars. Therefore we might hope to probe the mass function of stars in the lens galaxy by comparing the microlensing at different times or source sizes.

The notion of using multiple source sizes to “map out” lens mass distributions on various scales has been explored for quasar lensing by Metcalf et al. (2004) and Dobler & Keeton (2005). In particular, Dobler & Keeton plotted curves of magnification versus source size and pointed out that multiwavelength observations of quasar lenses could measure these curves. However, with quasar lenses it is possible to obtain only a few discrete points on the curves, say for X-ray, optical, and radio wavelengths, and there is no clear mapping between the observable quantity (wavelength) and source size. With SNe, by contrast, there is a simple mapping between the observable quantity (time) and the source size via the photosphere expansion rate. Furthermore, with good time sampling it would be possible to measure the entire magnification versus source size curve.

Of course, seeing microlensing in SN light curves is contingent upon having a SN expansion rate that is neither too large (which would “wash out” microlensing effects

at early times) nor too small (which would mean that the SN remains effectively a point source for its observable lifetime). In §2 we examine the typical SN expansion rate in units that are meaningful for microlensing, and estimate the optical depth for microlensing by stars in both the lens and host galaxies. In §3 we describe our microlensing simulations, and in §4 we show sample microlensed SNe light curves. In §5 we interpret the light curves and consider whether microlensing fluctuations could be used to extract information about the stellar population: the relative abundances of stars and smooth dark matter at the image positions, and the mass function of stars. We also consider whether microlensing will affect time delay measurements in lensed SNe, which have been proposed as a tool for precise measurements of H_0 (Oguri & Kawano 2003). Finally, in §6 we summarize our findings and discuss possibilities for future theoretical and observational advances.

2. THEORETICAL BACKGROUND

2.1. SN model

For our microlensing calculations, we model the source SN as an expanding disk of uniform brightness, taking as motivation the success of the Expanding Photosphere Method (EPM) originally developed by Kirshner & Kwan (1974). EPM assumes that the light emanating from a SN II explosion is due to a spherically symmetric, expanding hydrogen shell. The method (or closely related variants) has been used by several authors to estimate distances to observed SNe II (Kirshner & Kwan 1974; Schurmann, Arnett, & Falk 1979; Branch et al. 1983; Branch 1987). The efficacy of EPM rests on two assumptions: the photosphere is spherical and emits light with a Planck spectrum. Asphericity has been measured to be $< 30\%$ via spectropolarimetry (Leonard et al 2001), and departures from Planckian emission due to flux dilution has been studied numerically (Hershkowitz et al 1986; Hershkowitz & Wagoner 1987). Lastly, for this pilot study we also assume that the effects of limb darkening may be neglected.

2.2. Microlensing scale

It is important to ask how the size of the SN photosphere compares to scales relevant for microlensing during the SN’s observable lifetime. Given a population of stars in the lens galaxy, the relevant length scale for microlensing is the Einstein radius

$$\bar{R} = \left(\frac{4G\bar{m}}{c^2} D \right)^{1/2} \quad (1)$$

associated with the mean stellar mass \bar{m} . The distance factor D is a function of lens and source redshifts (z_l and z_s respectively) and cosmology. Throughout this paper we use $z_l = 0.32$ and $z_s = 0.53$, which represent the mean lens and source redshifts of the SLACS sample, and we take $\Omega_M = 0.3$, $\Omega_{\Lambda} = 0.7$, and $H_0 = 70$ km/s/Mpc. With these parameters, equation (1) gives

$$\bar{R} = 13.1 \left(\frac{\bar{m}}{M_{\odot}} \right)^{1/2} \text{ lt-day}. \quad (2)$$

To compare this with the size of the SN, we must convert the photosphere’s expansion rate into units of

³ The situation is similar to nanolensing of gamma ray bursts as explored by Walker & Lewis (2003).

the Einstein radius. If the edge of the photosphere is traveling at a velocity $v = 15,000 \text{ km/s} = 0.05 c$ (Eastman, Schmidt, & Kirshner 1996), this expansion rate is

$$\frac{dR}{dt} = \frac{v}{R} \bar{R} = 0.0038 \bar{R} \text{ day}^{-1}, \quad (3)$$

implying that the size of the SN is less than or comparable to \bar{R} for its observable lifetime ($t \sim 300$ days). In other words, the SN has a size that should make it quite sensitive to microlensing.

2.3. Estimates of self-lensing

Before examining microlensing by stars in an intervening lens galaxy, it is interesting to consider whether SNe (both lensed and unlensed) could be microlensed by stars *in their own host galaxies*. While this effect has yet to be identified in known SNe, the large SN catalogs that will be produced by SNAP may reveal effects that are rare. If we imagine that a SN goes off at the “back” (relative to the observer) of its host galaxy, we can estimate the self-lensing optical depth⁴ by integrating along the line of sight through the host galaxy,

$$\kappa_* = \int_0^{2L} n \pi R^2 dl, \quad (4)$$

where $2L$ is the diameter of the host galaxy, n is the number density of stars, and R is again the Einstein radius of an individual star. To make a simple toy model, we assume that n is constant through the galaxy, that all of the stars have the same mass m , and that the galaxy can be approximated as a sphere of radius L .

From the definition of the Einstein radius, equation (4) can be written as

$$\kappa_* = \int_0^{2L} n \frac{4\pi Gm}{c^2} \frac{d_l d_{ls}}{d_s} dl, \quad (5)$$

where d_l is the distance to the lens, d_s is the distance to the source, and d_{ls} is separation between the lens and the source. Since the distance to the host galaxy will be much larger than the galaxy itself, $d_s \approx d_l$ and $d_{ls} = l$. Integrating then yields

$$\kappa_* \sim \frac{6Gm_{gal}}{c^2 L}, \quad (6)$$

where we have used the fact that $nm = \rho$ is the mass density of the galaxy, and we have assumed a uniform spherical galaxy so $\rho \sim (3m_{gal})/(4\pi L^3)$ where m_{gal} is the total *stellar* mass in the galaxy. Note that the self-lensing optical depth is independent of the distance to the host galaxy. Using typical values for a Milky Way type galaxy, $m_{gal} \sim 10^{11} M_\odot$ and $L \sim 15 \text{ kpc}$, we find

$$\kappa_* \sim 2 \times 10^{-6}. \quad (7)$$

We conclude that the optical depth is too small, even for a SN at the back of the galaxy, to produce a significant number of self-lensing events even in the large catalogs that will be produced by SNAP.

⁴ Following the standard convention (Vietri & Ostriker 1983; Pacynski 1986; Kayser, Refsdal, & Stabell 1986; Wyithe & Turner 2001), we define the microlensing optical depth to be the fraction of the image plane area covered by the Einstein disks of stars. This is equal to the convergence κ_* , or the surface mass density of stars in units of the critical density for lensing.

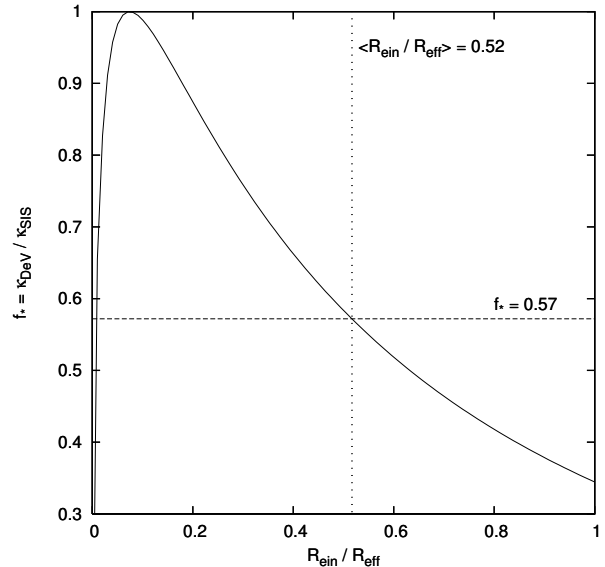


FIG. 1.— Maximum f_* as a function of $R_{\text{ein}}/R_{\text{eff}}$ assuming a de Vaucouleurs profile for the light and an isothermal profile for the mass. Koopmans et al. (2006) measure $\langle R_{\text{ein}}/R_{\text{eff}} \rangle = 0.52$ for the SLACS lenses. The maximum surface density in stars at that radius is $f_* = 0.57$.

2.4. Stellar mass fraction

The microlensing optical depth is characterized by the convergence κ_* , or the surface mass density of stars in units of the critical density for lensing (see Vietri & Ostriker 1983; Pacynski 1986; Kayser, Refsdal, & Stabell 1986; Wyithe & Turner 2001). It is convenient to define the fraction of the surface density in stars, $f_* = \kappa_*/\kappa_{\text{tot}}$, at the image positions. To make a rough estimate of f_* , we model the lens galaxy’s total mass distribution as a Singular Isothermal Sphere (see Koopmans et al. 2006),

$$\kappa_{SIS} = \frac{R_{\text{ein}}}{2r}, \quad (8)$$

where R_{ein} is the Einstein radius. We model the stellar mass distribution with a de Vaucouleurs model,

$$\kappa_{DeV} = A e^{-k(r/R_{\text{eff}})^{1/4}}, \quad (9)$$

where R_{eff} is the effective radius, and $k = 7.67$. If we set the stellar mass-to-light ratio equal to its maximum possible value such that $\kappa_{DeV} \not> \kappa_{SIS}$ for all r , we can find the maximum value of the normalization constant A . With this maximum value of A we can obtain an upper bound on $f_* = \kappa_{DeV}/\kappa_{SIS}$ as a function of radius.

Figure 1 shows the upper limit on f_* at the Einstein radius, as a function of $R_{\text{ein}}/R_{\text{eff}}$. The average Einstein radius of the SLACS lenses is $\langle R_{\text{ein}}/R_{\text{eff}} \rangle = 0.52$ (Koopmans et al. 2006), and this corresponds to a maximum stellar mass fraction of $f_* = 0.57$. Also interesting to consider is the integrated stellar mass fraction within the Einstein radius. We find the maximum value of this integrated stellar mass fraction to be 0.83 for $\langle R_{\text{ein}}/R_{\text{eff}} \rangle = 0.52$. For comparison, Koopmans et al. (2006) find the mean integrated stellar mass fraction to

be 0.75 for the SLACS lenses, suggesting that the actual stellar mass density is $\sim 90\%$ of its maximum possible value. This would imply that $f_* = 0.46$ at the Einstein radius (again for $\langle R_{\text{ein}}/R_{\text{eff}} \rangle = 0.52$). Therefore, we consider $f_* \approx 0.5$ to be a reasonable estimate of the stellar mass fraction near the image locations of the SLACS lenses

3. MICROLENSING SIMULATIONS

We model the population of stars using a Salpeter mass function, $dn/dm \propto m^{-2.35}$, spanning the mass range from m_1 to m_2 . We find it convenient to specify the mass range by setting the mean mass to be $\bar{m} = M_\odot$ and quantifying the dynamic range with $q = m_1/m_2$. Several authors have shown that microlensing magnification distributions are insensitive to the mean mass \bar{m} (Wyithe & Turner 2001; Schechter et al. 2004; Mortonson et al. 2004). For microlensing of SN light curves, the mean mass does set an overall time scale: as \bar{m} increases, the time it takes for the source to reach a given fraction of \bar{R} scales as $\bar{m}^{1/2}$.

The properties of the microlensing fluctuations should be dependent on the stellar population parameters (namely f_* and q). They also depend on the particular configuration of stars, because as shown in Figure 2 different realizations of stellar populations that are statistically equivalent yield very different magnification maps in the source plane. Note that these magnification maps are $2.5\bar{R}$ on a side, so a SN will expand to cover roughly half of a map during its observable lifetime.

We compute microlensing magnifications using a new ray-shooting code. The code uses a simplified version of a tree algorithm to efficiently compute deflection angles for a population of stars. Whereas the ray-shooting algorithm used by Wambsgans (1999) is designed to provide magnifications for many source positions (yielding magnification maps), our new algorithm is optimized for handling a wide range of source sizes. Details of the code will be presented elsewhere (Dobler & Keeton, in prep.).

4. RESULTS

In our first set of simulations we set $\kappa = \gamma = 0.45$, where $\kappa = \kappa_* + \kappa_s$ is the total surface mass density, κ_s is the surface density of a smooth dark matter component, and γ is the external shear. We choose $\kappa = \gamma = 0.45$ for illustrative purposes as these are typical values for a positive parity image near the Einstein radius of an isothermal lens galaxy. In the absence of microlensing (i.e., if there were only “macrolensing” due to the lens galaxy), this would yield a magnification of $\mu_0 = 10$.

Initially we isolate microlensing fluctuations by plotting the *difference light curve*,

$$\Delta M(t) = -2.5 \log \left[\frac{I(t)}{\mu_0 S(t)} \right], \quad (10)$$

where $S(t)$ and $I(t)$ are the intrinsic and observed brightnesses of the SN. This definition is chosen so that $\Delta M = 0$ in the absence of microlensing. In general we expect $\Delta M(t) \rightarrow 0$ as $t \rightarrow \infty$ since large sources are insensitive to microlensing. Figure 3 shows a sample difference light curve for one stellar realization with a uniform mass function ($q = 1$) and 100% of the surface density in stars ($f_* = 1$). Over the observable lifetime of the SN, this stellar configuration creates an *offset* of up to 0.75 mag,

and *fluctuations* at the level of 0.1–0.2 mag. These effects are well within the realm of detectability.

We now combine difference light curves with data for the observed SN 2004ej from the Carnegie Supernova Project (CSP)⁵. SN 2004ej is a classic example of a SN II-P (plateau) in which the light curve falls off slowly at early times, drops suddenly by almost 2 mag, and then decreases slowly thereafter. Figure 4 shows four examples of microlensing effects. Depending on the specific stellar configuration, the SN light curve can be changed either subtly or dramatically. In particular, panel (a) shows a large offset due to microlensing, plus small-amplitude fluctuations. Panel (b) shows not only an offset of ~ 1 mag, but also a pronounced peak that is not present in the intrinsic light curve. The ability of microlensing to induce such large-scale features may limit the precision with which one can “match up” light curves from different lensed images to measure precise lensing time delays (see §5.2). Panel (c) shows that the microlensing fluctuations can be more subtle with only small fluctuations about the intrinsic light curve, while panel (d) shows that microlensing can substantially alter the decay rate of the SN light curve.

The lensed image configurations for various epochs of panel (b) are shown in Figure 5. Even when the SN is small there are multiple micro-images, and no single image is dominant. As the SN expands, more and more small micro-images appear, and a few larger micro-images near the center begin to merge. The distribution of micro-images is elongated along the shear axis (the horizontal axis in Fig. 5). Even at $t = 200$ days ($R_{\text{src}} = 0.76R_{\text{ein}}$), by which time several merged images have formed, there is still no clear “primary” micro-image. The complexity of the image configurations is striking and attests the richness of the phenomenon.

Figure 6 shows difference light curves for various random star populations (all with $q = f_* = 1$). It is clear that *all* of the realizations produce offsets, which can be as large as 1–1.5 mag. The amplitude of the smaller scale fluctuations depends on the timescale. That is, there are occasionally very rapid variations at the level of ~ 0.2 mag, while longer time scale variations can be as large as ~ 0.5 –1.0 mag. To test if these trends are specific to these particular stellar population parameters, Figure 7 shows the effects of varying q and f_* . We show 10 realizations of the stellar population for each parameter combination. It is clear that microlensing fluctuations are very generic. While at first glance it is not obvious whether the realizations differ substantially from one panel to another, each *individual* curve has an enormous amount of structure. It would seem that a lot of information about the stellar population is hidden in the light curves; the challenge is figuring out how to extract it (see §5.1).

Figure 7 also shows that there is not a single realization that does *not* produce fluctuations over the lifetime of the SN. To quantify this point, we define

$$\Delta_{\text{max}} = \max(\Delta M(t)) - \min(\Delta M(t)) \quad (11)$$

to measure the overall change in any difference curve. Figure 8 shows the probability distribution for Δ_{max} .⁶

⁵ <http://csp1.lco.cl/~cspuser1/CSP.html>

⁶ We have combined all stellar population parameters and configurations. While this does wash out detailed information that

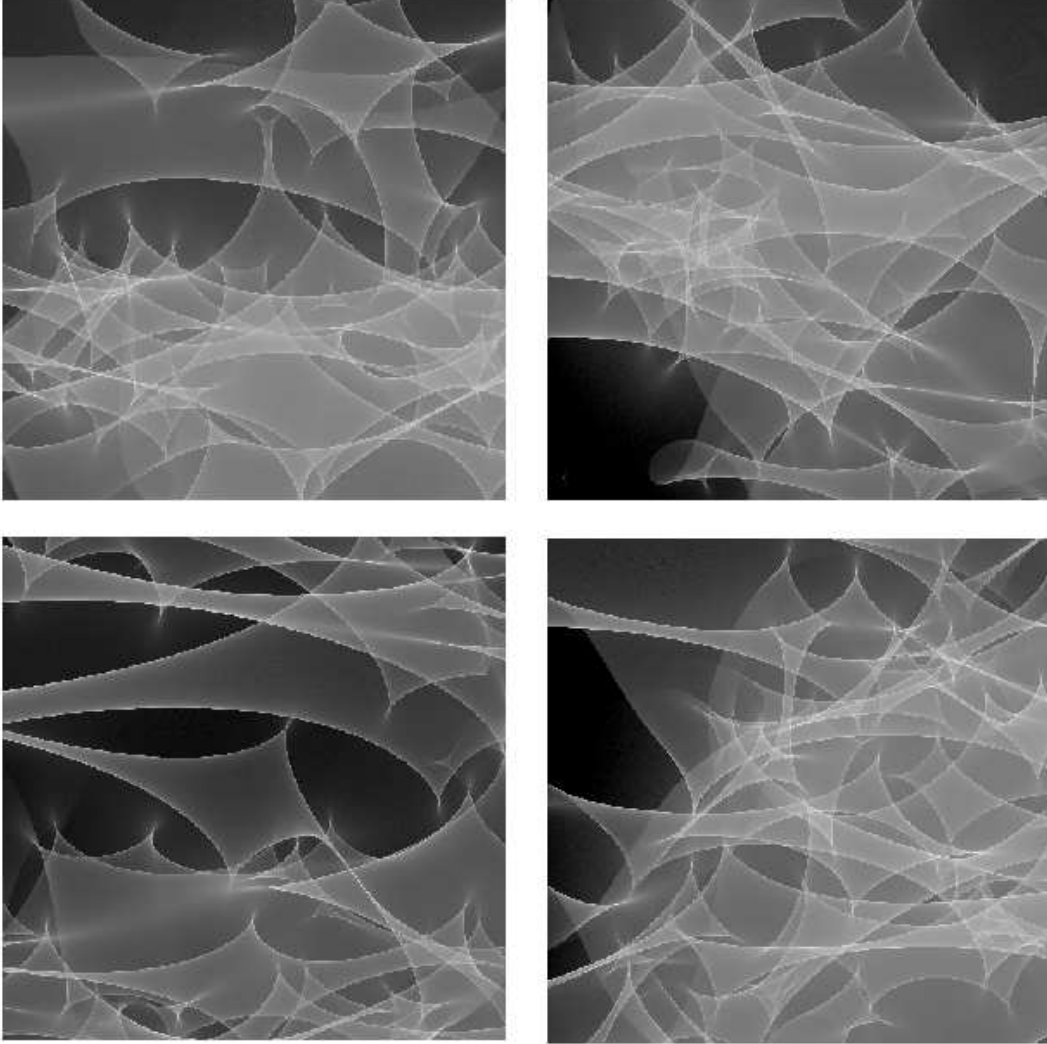


FIG. 2.— Sample magnification maps for four different realizations of stellar populations with $f_* = q = 1.0$ and $\bar{m} = M_\odot$. (These maps were generated with the code by Wambsganss (1999), although we actually use our own microlensing code to compute SN light curves.) The side length of each map is $2.5R$, so an expanding SN will grow to cover approximately one half of a map. The large qualitative differences in the magnification maps imply that microlensing fluctuations will be very different from one SN light curve to the next, even for fixed stellar population parameters.

There are two crucial points. First, the Δ_{\max} distribution is not peaked at zero, so microlensing fluctuations are more likely than not to be observed in SN light curves. Second, the total variation in a given SN light curve due to microlensing can be quite large. The Δ_{\max} distribution is peaked at ~ 0.6 mag with a long tail that extends to > 2 mag. Strikingly, the probability that Δ_{\max} is less than ~ 0.1 mag is quite low. From the cumulative distribution, we estimate that 70% of lensed SN light curves will have microlensing fluctuations greater than 0.5 mag, and 25% will have fluctuations greater than 1 mag. We have checked that similar conclusions hold for other typical values of κ and γ (specifically, those used in §5.2),

may distinguish one set of stellar population parameters from another, for the moment we only seek to understand how likely it is that microlensing fluctuations will be seen in a lensed SN. We have examined Δ_{\max} distributions for different stellar populations, and they are all qualitatively similar to the distribution shown in Figure 8.

including both positive and negative parity situations.

The implication is that microlensing of lensed SNe is almost a certainty given reasonable stellar populations.

5. ANALYSIS

5.1. *Extracting parameters of the stellar population*

Comparing the various panels of Figure 7, the eye picks out some qualitative features. For example, in the $q = 0.01$ cases there seem to be more regions where the difference light curves are fairly flat than in the $q = 1.0$ cases. To quantify this feature, we compute the time-weighted derivative (TWD) of the difference light curves,

$$\text{TWD} = -t \times \frac{\partial}{\partial t} \Delta M, \quad (12)$$

where the negative sign ensures that TWD is positive for increasing brightness (i.e., decreasing magnitude). It is useful to explain the motivation further. When the mass range is broad (q is small), there are a few high-mass

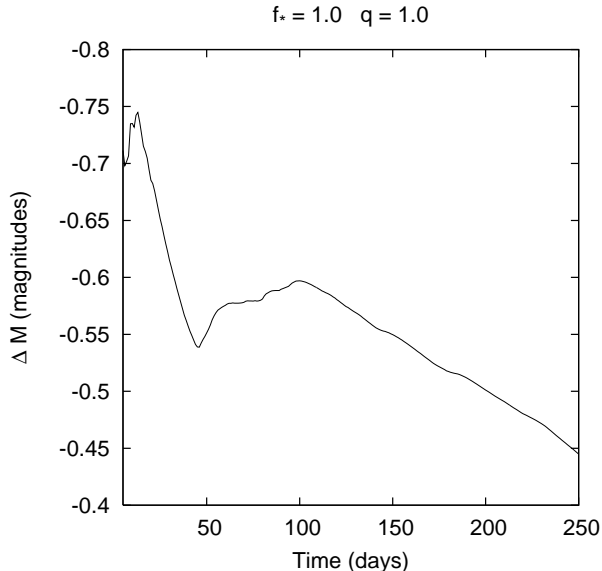


FIG. 3.— A sample difference light curve for SN microlensing with a uniform mass function ($q = 1$) and 100% of the surface density in stars ($f_* = 1$). Microlensing produces offsets of nearly 1 mag, and shorter time scale fluctuations as large as 0.1–0.2 mag.

stars and they tend to be well separated. When the photosphere encounters one of these stars there can be an abrupt change in the lensing magnification which leads to a “step” in the light curve. Conversely, between these abrupt events the magnification fluctuations are small. A similar argument holds when the stars are diluted by a smooth mass component (f_* decreases). While different stellar configurations certainly produce different light curves, in general the step-type fluctuations are more characteristic of low q or low f_* . The time-weighting of the derivative accounts for finite source effects: the change in brightness will happen over a longer time scale when a larger source comes into contact with a stellar caustic.

The TWD curves are shown in Figure 9. There is striking contrast among the different f_* and q combinations. In general, the $q = 0.01$ cases do seem more tightly bound about $\text{TWD} = 0$ (i.e., flat difference light curves); this effect is particularly notable for $f_* = 0.2$. There is an even more pronounced effect when comparing different f_* values at fixed q . Diluting the stellar component with smooth dark matter clearly *increases* the scatter about $\text{TWD} = 0$.

Notice that the TWD curves show large positive spikes, but no corresponding negative spikes. This is because there is a simple lower bound on the TWD, which can be seen as follows. The difference light curve may be written as

$$\Delta M = -2.5 \log \left[\frac{A_I}{\mu_0 \pi R_{\text{src}}^2} \right], \quad (13)$$

where A_I is the area of the images. Therefore the TWD is

$$\text{TWD} = \frac{2.5 t}{\ln(10)} \left[\frac{1}{A_I} \frac{\partial A_I}{\partial t} - \frac{2}{R_{\text{src}}} \frac{\partial R_{\text{src}}}{\partial t} \right]. \quad (14)$$

For linear expansion $R_{\text{src}} = vt$ so the second term simplifies and we obtain

$$\text{TWD} = \frac{2.5 t}{A_I \ln(10)} \frac{\partial A_I}{\partial t} - \frac{5}{\ln(10)}. \quad (15)$$

In the first term, it is important to understand that $\partial A_I / \partial t \geq 0$. This is because as the source expands and crosses more and more caustics, images can never disappear. Distinct images may merge, but they cannot vanish because, if a particular source position is covered by the photosphere at one time, it is covered at all later times as well.⁷ This means that the first term is non-negative, so we have $\text{TWD} \geq -5 / \ln(10) = -2.17$. In practice, our TWD curves do not even dip below $\text{TWD} \approx -1$, which suggests that there may be some other effect bounding the TWD. Nevertheless, this argument does explain why there are no large negative spikes, only large positive spikes.

To quantify our sense that different stellar populations have TWD curves that are more or less tightly bound around zero, we compute the dispersion in the TWD distribution averaged over all times and all curves for each panel in Figure 9. Figure 10 shows how the TWD dispersion depends on f_* for the various values of q . We find a clear decrease in the TWD dispersion as f_* increases. There is no obvious trend with q . We conclude that the TWD contains key information about the relative amounts of stellar versus smooth dark matter mass densities. Constraints on the stellar mass function will be more difficult to extract from the TWD, but perhaps other statistical measures can be found that will reveal information about the mass function.

5.2. Time delay uncertainties

One goal for lensed SNe is to measure lensing time delays very precisely. We now consider whether microlensing may make it difficult to “match up” light curves to determine the time delay. To consider a realistic lensing scenario, we consider the SLACS lens SDSS J2300+0022 and use the lens model by Koopmans et al. (2006). We place a SN near the center of the source and solve the lens equation to find the local convergence and shear at the two SN image positions ($\kappa = \gamma = 0.39$ for the positive parity image and $\kappa = \gamma = 0.52$ for the negative parity image), and also the time delay between the images ($\Delta t_0 = 16.5$ days). We then generate mock light curves starting from two observed cases: SN 2004ej and SN 2004ex from the CSP. We seek to focus on the uncertainties induced by microlensing, so we limit the uncertainties due to finite sampling by artificially boosting the time sampling to ~ 4 hours with linear interpolation. We generate microlensing difference curves using $f_* = 0.5$ (see §2.4), a uniform mass function ($q = 1.0$), and then add them to the intrinsic light curves to obtain different realizations of lensed SN light curves. We create 20 random realizations for each image, which can be used to construct 400 distinct “observations.”

For each “observation,” we then attempt to recover the time delay by matching up the light curves from the two

⁷ The surface brightness of the photosphere may change with time, but that does not affect our argument because in equations (13) and (14) we only need to specify the *area* of the images; the source surface brightness has factored out.

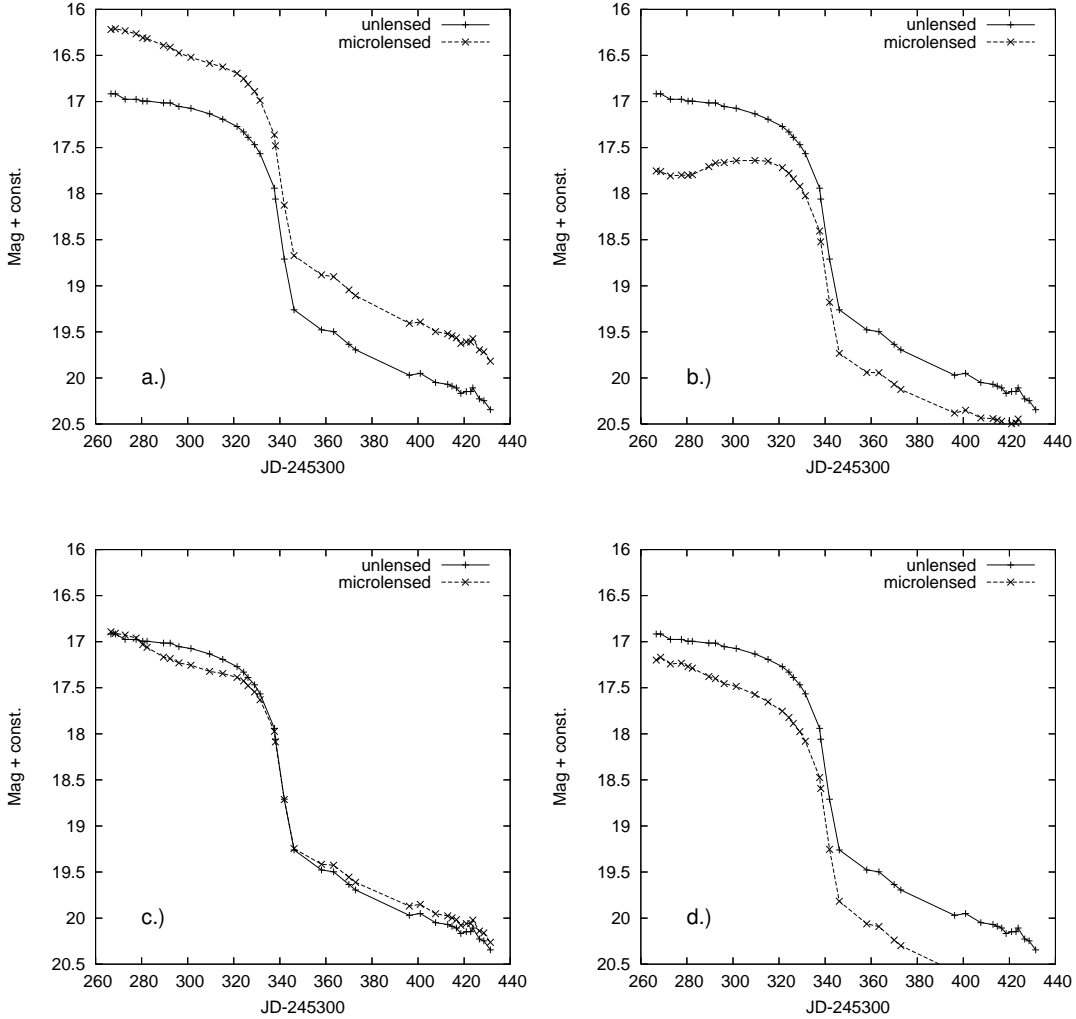


FIG. 4.— Sample light curves for SN 2004ej, both with (dashed) and without (solid) microlensing fluctuations. The intrinsic light curve data are taken from the Carnegie Supernova Project. The four panels represent different stellar configurations which lead to numerous qualitative changes in the observed light curve. Microlensing can produce (a) a large offset, (b) non-intrinsic features such as peaks, (c) small fluctuations, or (d) changes to the decay rate.

images. Specifically, we minimize the goodness of fit

$$\chi^2(\Delta t) = \frac{1}{N} \sum_{i=1}^N \frac{1}{\sigma_i^2} [D^+(t_i) - D^-(t_i - \Delta t) - k]^2. \quad (16)$$

Here D^+ and D^- are the positive and negative parity SN light curves (in magnitudes), respectively. The normalization constant k is required because the two images have different *macro*-magnifications from the main lens galaxy; in the absence of microlensing, $k = -2.5 \log(\mu_+/\mu_-)$. Also, N is the number of data points for which the shifted light curves overlap. We normalize χ^2 by N in order to avoid a scenario in which the optimization routine takes χ^2 to zero simply by shifting the light curves so they do not overlap and there are no terms in the sum. For simplicity, we assume that the photometric uncertainties σ_i are Gaussian and constant in time.

Figure 11 shows sample observations, together with histograms of the recovered time delays. The time delay

histograms are broad: the dispersions are $\sigma = 1.5$ days for SN 2004ej and 3.6 days for SN 2004ex, implying that microlensing will make it difficult to measure time delays more precise than a few days. Furthermore, the Δt histograms are peaked not at the true time delay but rather at a higher value, and are significantly skewed.

The differences between the results for the two different intrinsic SNe can be understood by comparing the intrinsic light curves. SN 2004ej has a very distinct, large amplitude intrinsic feature at $t \approx 340$ days. The light curve decreases rapidly by ~ 2 mag, which is larger than typical microlensing effects (see Fig. 7). In this case, microlensing can perturb the time delay analysis but cannot fundamentally disrupt the ability to line up the light curves and measure the time delay. Conversely, SN 2004ex has intrinsic variability over longer time scales and, more importantly, of smaller amplitude. Microlensing introduces fluctuations with similar time scales and amplitudes, which makes it considerably more difficult to match up the light curves of the two images.

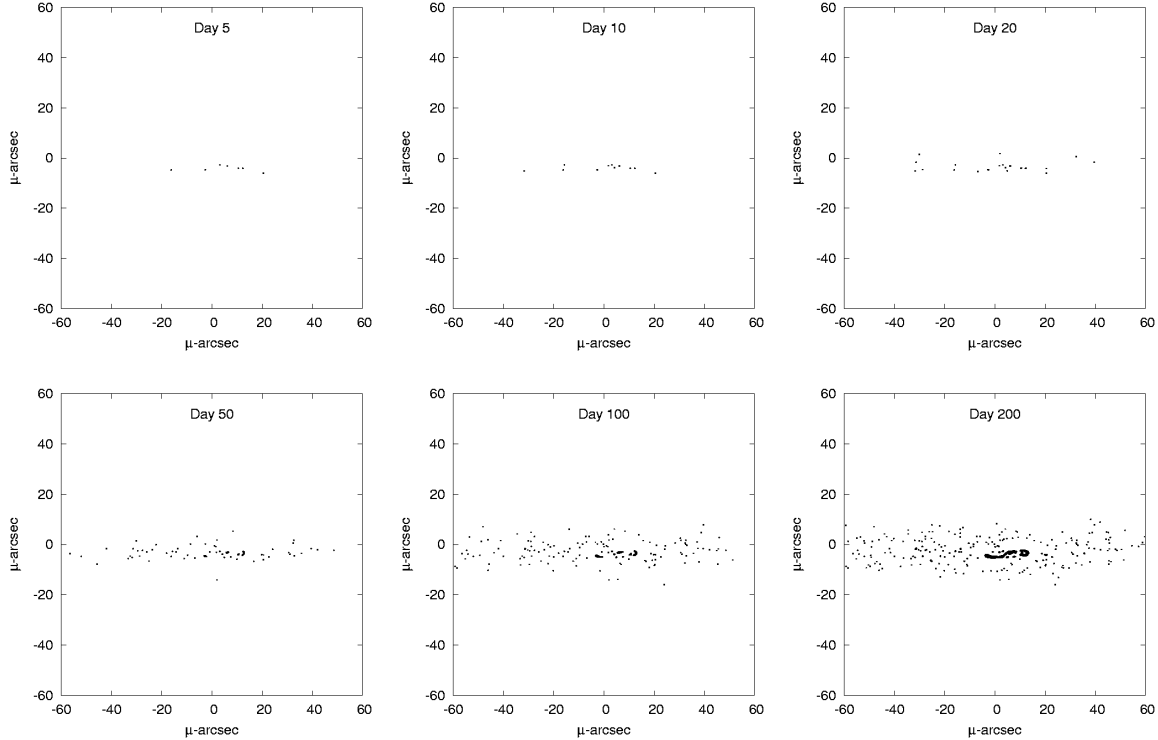


FIG. 5.— Micro-image configurations at various epochs for $q = f_* = 1.0$. As the SN grows in size, micro-images appear and merge. The source size of the photosphere for these image configurations is $R_{\text{src}} = 0.019, 0.038, 0.076, 0.19, 0.38,$ and $0.76 R_{\text{ein}}$ for times $t = 5, 10, 20, 50, 100,$ and 200 days respectively. The photometric effects on the intrinsic SN light curve for this particular stellar configuration are shown in panel (b) of Figure 4.

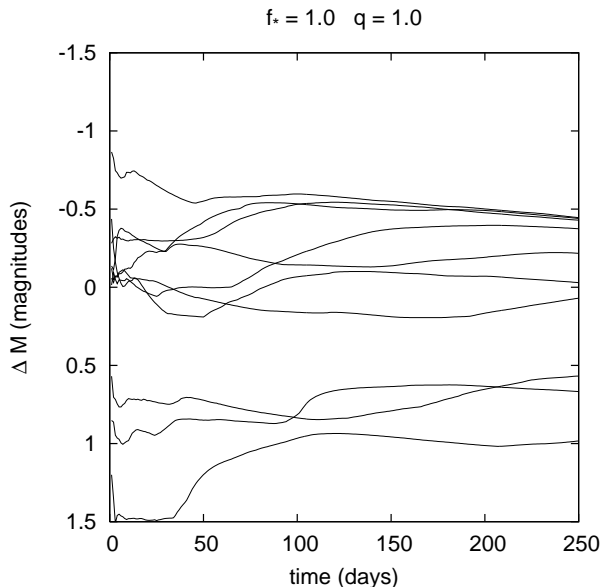


FIG. 6.— Difference light curves for fixed $f_* = q = 1.0$ but varying stellar configurations. Short time scale fluctuations ~ 0.2 mag are quite common, while longer time scale variations can be as large as 0.5 – 1.0 mag.

We consider whether it is possible to improve the time delay measurements by “masking out” portions of the

light curve when the source is more susceptible to microlensing. Specifically, we repeat the time delay analysis while ignoring the first 25% of the light curve when the source is small and microlensing fluctuations are largest, and the last 25% when the source is becoming faint. For SN 2004ej this effectively isolates the large intrinsic drop around $t \approx 340$ days, and leads to a smaller time delay dispersion of $\sigma = 0.6$ days. In other words, if the light curve has a strong intrinsic feature, it can pay to focus on this feature for measuring the time delay. For SN 2004 ex, by contrast, masking the first and last parts of the light curve leads to a larger dispersion of $\sigma = 4.40$ days. This is not surprising since, with no dominant intrinsic feature, masking out part of the data only serves to decrease the number of data points.

In other words, the extent to which microlensing corrupts time delay measurements will depend on whether there are strong intrinsic features in the SN light curve. Of course, for a real lensed SN the intrinsic light curve will not be known, and the challenge will be to determine which observed features are intrinsic and which are due to microlensing effects. Nevertheless, we can conclude in general that microlensing effects must be taken into account when attempting to extract high precision time delays from multiply imaged SNe.

6. CONCLUSIONS

In anticipation of the discovery of lensed SNe in the near future with SLACS and SNAP, we have undertaken a pilot study of the fluctuations in the observed light curves due to microlensing by stars in the lens galaxy.

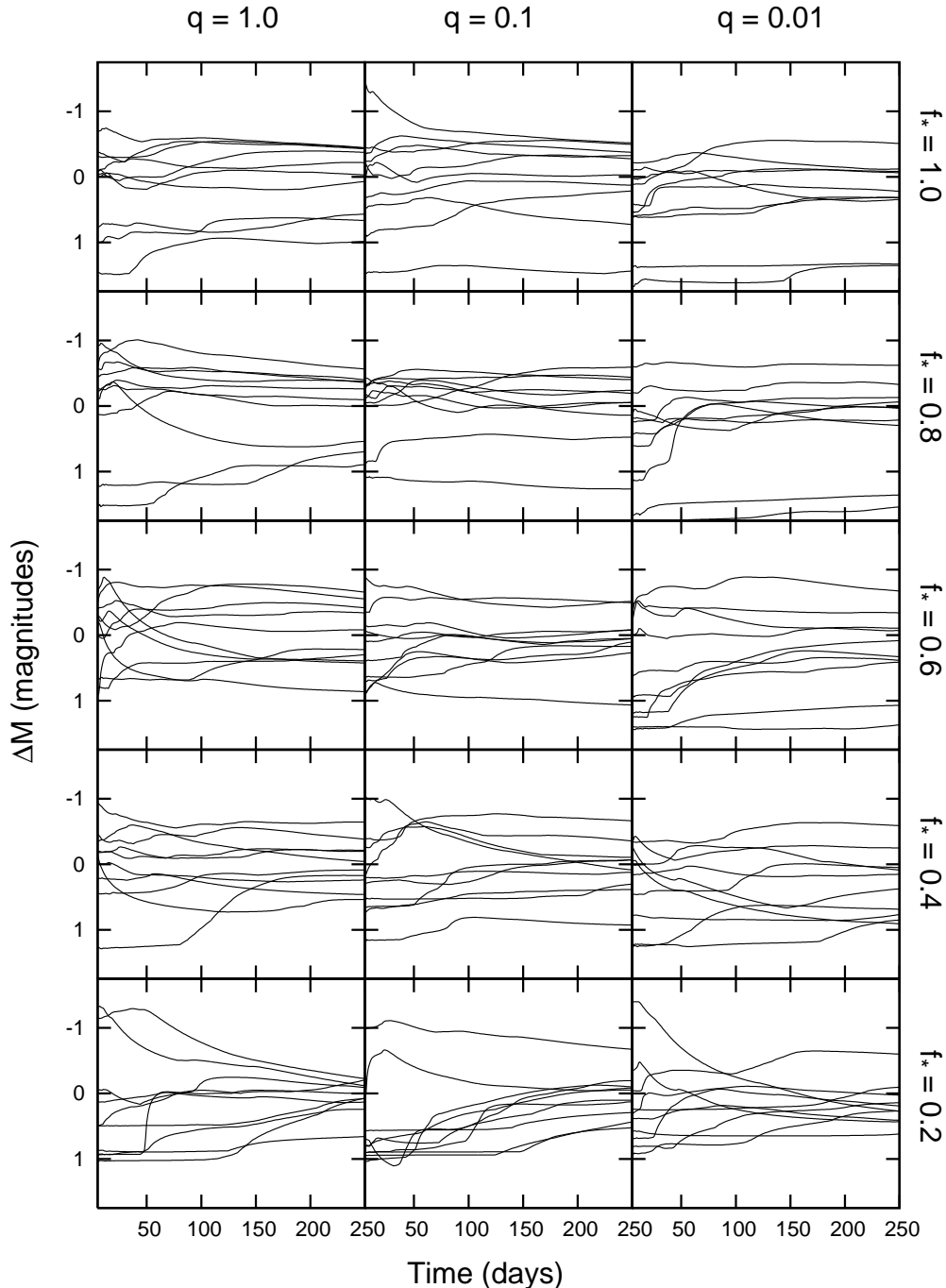


FIG. 7.— Difference light curves for various q and f_* . Ten realizations of the stellar configuration are shown for each case. Significant microlensing fluctuations are seen in every realization and for every combination of q and f_* , implying that microlensing will be quite common in lensed SNe.

Our main findings can be summarized as follows.

- The microlensing optical depth and the angular size of the source SN virtually ensure that microlensing fluctuations will be present in lensed SN light curves.
- Microlensing can produce an overall brightness offset of ~ 1 mag, short time scale brightness fluctuations of ~ 0.1 – 0.2 mag, and longer time scale fluctuations of ~ 0.5 – 1.0 mag.
- We estimate that $\sim 70\%$ of lensed SN light curves will have microlensing fluctuations larger than 0.5 mag, and $\sim 25\%$ will have fluctuations larger than 1 mag. The probability that microlensing effects will *not* be present in any given light curve is $\lesssim 5\%$.

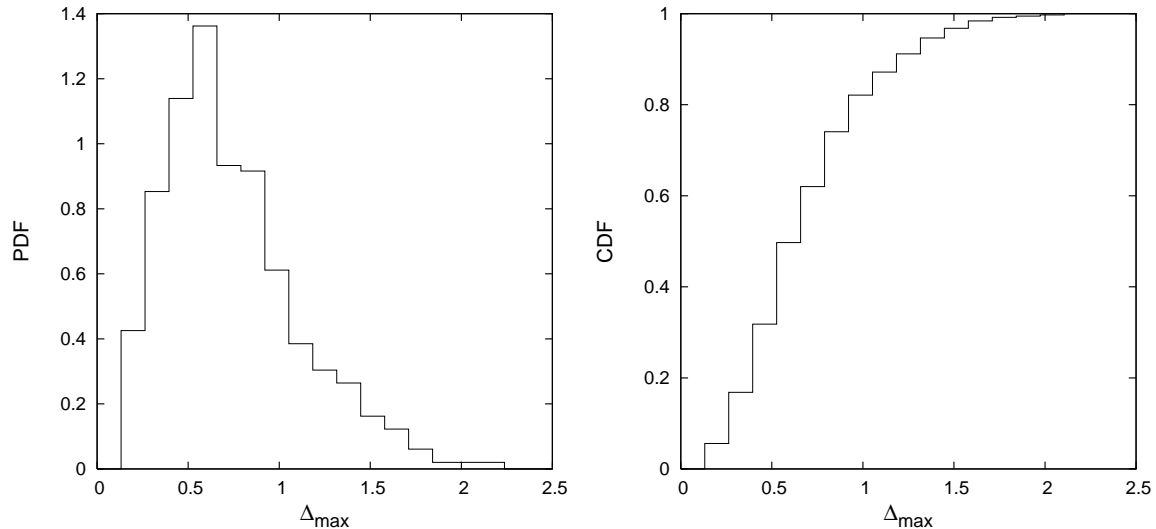


FIG. 8.— The probability density function (left) and cumulative distribution function (right) for Δ_{\max} , averaged over all stellar population parameters and configurations. The PDF is peaked at 0.6 mag with a long tail extending to > 2 mag. The CDF shows that roughly 70% of observed SN light curves will exhibit microlensing fluctuations > 0.5 mag, and 25% will show fluctuations > 1 mag.

- Microlensing fluctuations can generate dramatic and easily observable changes to the intrinsic SN light curve. These features will complicate efforts to use time delays to measure the Hubble constant to high precision. Without detailed knowledge of the intrinsic structure of the light curve, time delays accurate to better than a few days will be difficult to obtain.

We should say that if microlensing fluctuations are *not* observed in lensed SN light curves, there are two possible interpretations: either the ratio of stellar mass density to smooth dark matter mass density (at the image positions) is so low that the microlensing optical depth is near zero; or the SN photosphere undergoes an initial period of very rapid expansion ($v \gg 15,000$ km/s at early times).

The microlensing fluctuations depend on the stellar mass fraction and mass function in the lens galaxy, although there are such large difference between different random star configurations that it may be challenging to extract the stellar population parameters. We have introduced the time-weighted derivative (TWD) of the light curve as a quantity that may be useful for this analysis. The TWD is relevant because of the correlation between fluctuation time scales, stellar Einstein radii, and the photosphere expansion velocity. We find that TWD statistics may be most useful for determining the relative abundances of stars and dark matter at the image

positions. More generally, the amount of structure in the light curves is a sign that more effort should be exerted to figure out how to analyze lensed SN light curves to determine properties of the stellar population.

Once a lensed SN is typed via spectroscopy or the late-time shape of the photometric light curve, it may be possible to model the intrinsic light curve. The efficacy of EPM implies that the source geometry at different epochs in the observations will be fairly well known, and so a light curve fitting method (such as that described by Kochanek 2004) may ultimately be the best analysis. The fitting method must be extended to efficiently incorporate *expanding* sources as opposed to *moving* sources; however the basic idea of finding a family of possible stellar configurations and using a Bayesian likelihood analysis to extract mass function parameters will remain the same.

We thank Mark Phillips and the Carnegie Supernova Project for providing data for SN 2004ej and SN 2004ex. We thank Gary Bernstein and the anonymous referee for helpful comments and suggestions. CRK thanks Mike Gladders for stimulating discussions at the conception of this project. This project is supported by grant HST-AR-10668 from the Space Telescope Science Institute, which is operated by the Association of Universities for Research in Astronomy, Inc., under NASA contract NAS5-26555.

REFERENCES

- Aldering G. et al., 2004, astro-ph/0405232
 Bolton A. S., Burles S., Schlegel D. J., Eisenstein D. J., Brinkmann J., 2004, AJ, 127, 1860
 Bolton A. S., Burles S., Koopmans L. V. E., Treu T., Moustakas L., 2006, ApJ, 638, 703
 Branch D. et al. 1983, ApJ, 244, 780
 Branch D., 1987, ApJ, 320, L23
 Cooray A., Holz D. E., Huterer D., 2006, ApJ, 637, 77
 Dobler G., Keeton C. R., 2005, MNRAS, 365, 1243
 Dobler G., Keeton C. R., Wambsgans J., 2005, astro-ph/0507522
 Eastman R. G., Woosley S. E., Weaver T. A., Pinto P. A., 1994, ApJ, 430, 300
 Eastman R. G., Schmidt B. P., Kirshner R., 1996, ApJ, 466, 911
 Eisenstein D. J., Annis J., Gunn J. E. et al., 2001, AJ, 122, 2267
 Filippenko A. V., 1997, Ann. Rev. Astron. Astrophys., 35:309-55
 Hershkovitz S., Linder E., Wagoner R., 1986, ApJ, 301, 220
 Hershkovitz S., Wagoner R., 1987, ApJ, 322, 967

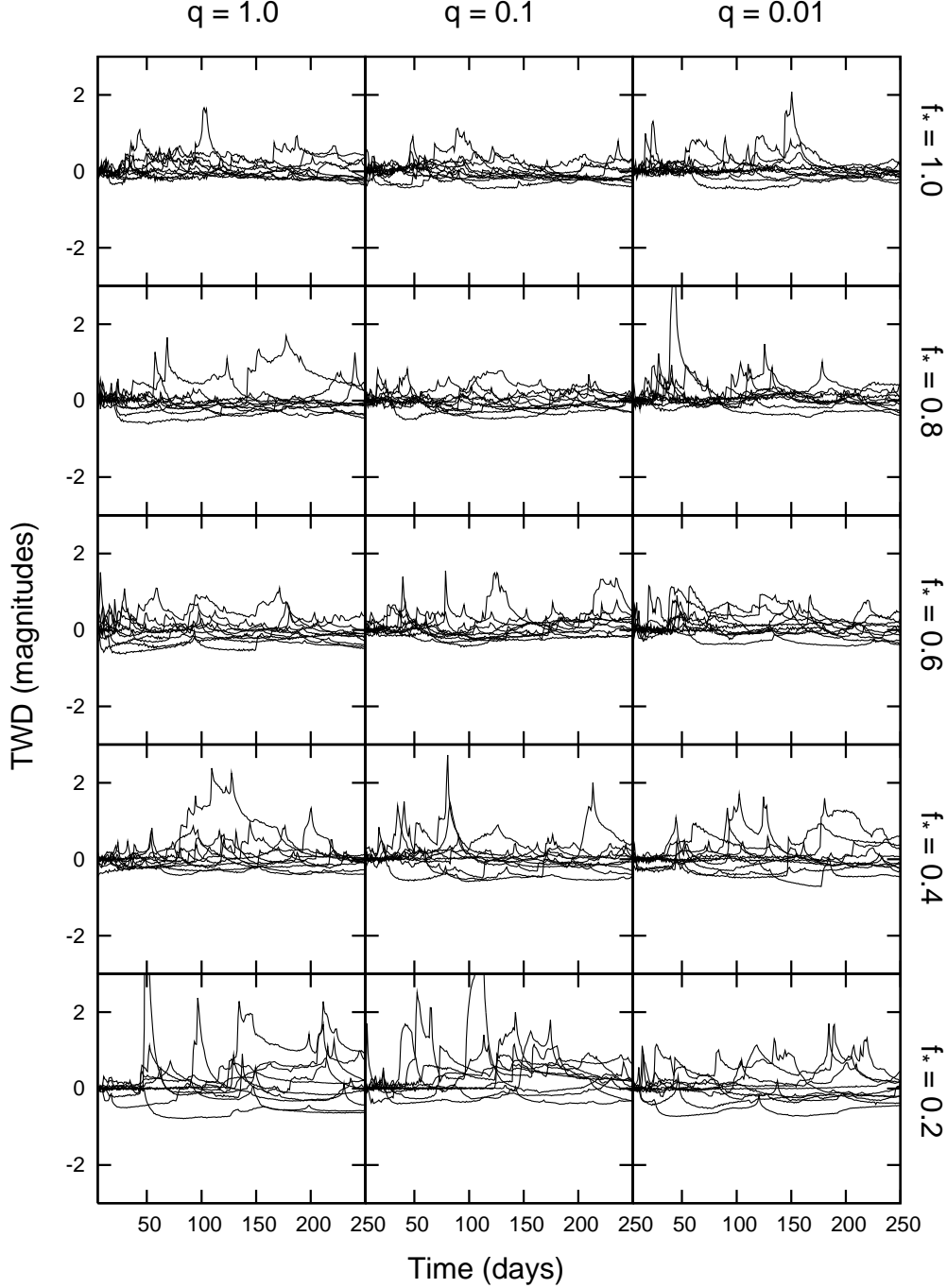


FIG. 9.— Time-weighted derivatives (TWD) of the difference light curves shown in Figure 7. In general, for fixed f_* the TWD is more tightly bound about zero for smaller values of q . This effect is more pronounced for fixed q and larger values of f_* .

Hogg D. W., Cohen J. G., Blandford R., Pahre M. A., 1998, *ApJ*, 504, 622
 Kayser R., Refsdal S., Stabell R., 1986, *AA*, 166, 36
 Keeton C. R., Burles S., Schechter P. L., Wambsganss J., 2006, *ApJ*, 639, 1
 Kenicutt R. C., 1992, *ApJ*, 388, 310
 Kirshner R. P., Kwan J., 1974, *ApJ*, 193, 27
 Knop R. A. et al. 2003, *ApJ*, 598, 102
 Kochanek C. S., 2004, *ApJ*, 605, 58
 Kolatt T., Bartelmann M., 1998, *MNRAS*, 296, 763

Koopmans L. V. E., Treu T., Bolton A. S., Burles S., Moustakas L.A., 2006, *astro-ph/0601628*
 Leonard D. C., Filippenko A. V., Ardila D. R., 2001, 553, 861
 Mannucci F. et al. 2005, *A&A*, 433, 807
 Metcalf R. B., Moustakas L. A., Bunker A. J., Parry I. R., 2004, *ApJ*, 607, 43
 Mortonson M. J., Schechter P. L., Wambsganss J., 2004, *astro-ph/0408195*
 Oguri M., Suto Y., Turner E. L., 2003, 583, 584
 Oguri M., Kawano, Y., 2003, *MNRAS*, 338, L25
 Pacynski B., 1986, *ApJ*, 301, 503

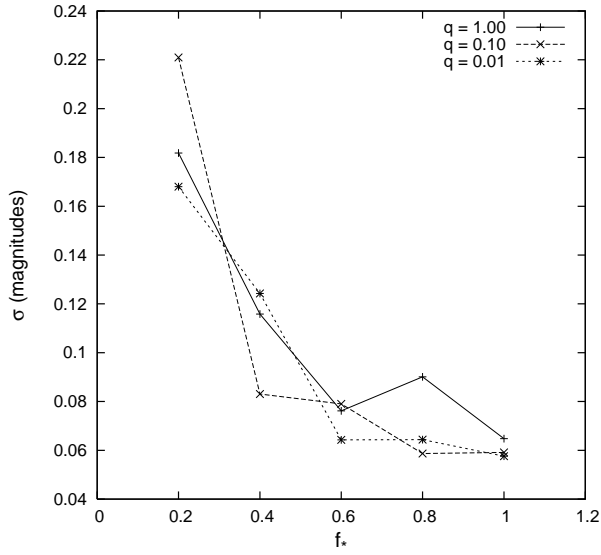


FIG. 10.— Dispersion σ in the TWD distributions, plotted versus f_* for the three values of q . There is a clear decrease of σ as f_* is increased from 0.2 to 1.0. Thus, microlensing fluctuations in SN light curves may be useful in extracting the relative amounts of stellar and smooth dark matter at the positions of the lensed images.

- Perlmutter S. et al. 1999, ApJ, 517, 565
 Riess A. G. et al. 1998, AJ, 116, 1009
 Riess A. G. et al. 2004, ApJ, 607, 665
 Schechter P. L., Wambsganss J., 2002, ApJ, 580, 685
 Schechter P. L., Wambsganss J., Lewis G. F., 2004, ApJ, 613, 77
 Schurmann S. R., Arnett W. D., Falk S. W., 1979, ApJ, 230, 11
 Spergel D. N. et al., 2003, ApJS, 148, 175
 Tonry J. L. et al. 2003, ApJ, 594, 1
 Treu T., Koopmans L. V. E., Bolton A. S., Burles S., Moustakas L., 2006, ApJ, 604, in press
 Vietri M., Ostriker J. P., 1983, ApJ, 267, 488
 Walker M. A., Lewis G. F., 2003, ApJ, 589, 844
 Wambsganss J., 1999, JCAM, 109, 353-372
 Woźniak P. R., Alard C., Udalski A., Szymański M., Kubiak M., Pietrzyński G., Zeburuń K., 2000, ApJ, 529, 88
 Wyithe J. S. B., Turner E. L., 2001, MNRAS, 320, 21
 Young T. R., Branch D., ApJ, 342, L79

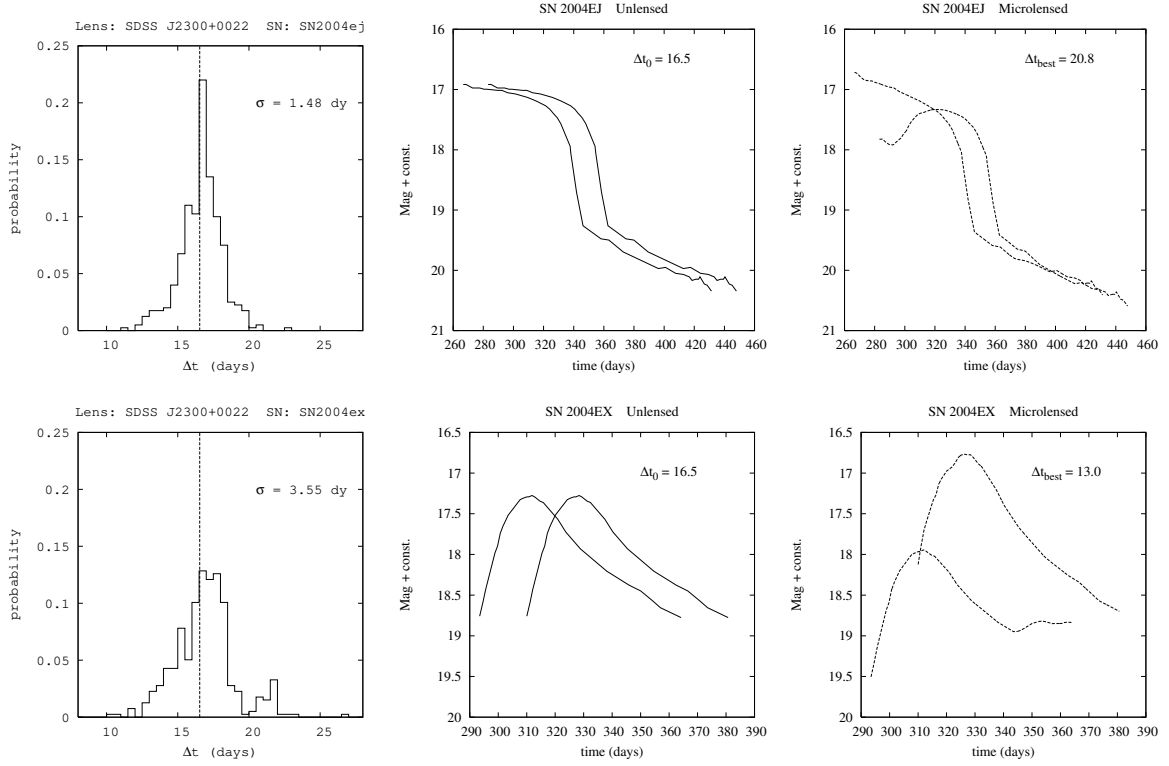


FIG. 11.— Illustration of the effects of microlensing on time delay measurements. We create a mock lensed SN using two different intrinsic SN light curves (SN 2004ej and SN 2004ex, both from the CSP) and lens/source parameters from the SLACS lens J2300+0022 (Koopmans et al. 2006). Left column: Histograms of the recovered time delays for 400 mock observations. The true time delay $\Delta t_0 = 16.54$ days is marked with a vertical line. The histograms are broad (dispersion $\sigma = 1.48$ days and 3.55 days for SN 2004ej and SN 2004ex respectively) and skewed with peaks offset from Δt_0 . The implication is that microlensing effects will render high precision time delays difficult to measure from multiply imaged SNe. Center column: The intrinsic light curves for the two SNe. The leading and trailing light curves correspond to the positive and negative parity images, respectively. Right column: The positive and negative parity light curves, including microlensing fluctuations, for one sample mock observation.